ELSEVIER

Tectonophysics 352 (2002) 203–224

TECTONOPHYSICS

www.elsevier.com/locate/tecto

High-temperature deformation in the Neoproterozoic transpressional Ribeira belt, southeast Brazil

Marcos Egydio-Silva [a,*], Alain Vauchez [b], Jérôme Bascou [a,b], João Hippertt [c]

[a] *Instituto de Geociências da Universidade de São Paulo, Rua do Lago 562, Cep: 05508-080, São Paulo, SP, Brazil*
[b] *Laboratoire de Tectonophysique, Université Montpellier II, 34095 Montpellier cedex 5, France*
[c] *Departamento de Geologia, Universidade Federal de Ouro Preto, 35400-000, Ouro Prêto, MG, Brazil*

Received 5 April 2001; accepted 12 December 2001

Abstract

The Neoproterozoic Ribeira belt is subdivided in two domains with contrasting tectonic characteristics. The northern domain is dominated by shallowly dipping foliations and orogen-normal thrust tectonics. The southern domain is characterized by a 1000-km-long network of anastomosing transcurrent shear zones parallel to the belt. This contrast is interpreted as reflecting continent–continent convergence that is almost orthogonal to the margins in the northern domain and significantly oblique in the southern domain. The central, transitional, domain of the Ribeira belt displays the northern termination of the transcurrent shear zone network: the Além Paraíba–Pádua shear zone system (APPSS). The 250-km-long Além Paraíba–Pádua system involves granulites facies mylonites deformed through transpression. A detailed study of the microstructure and lattice preferred orientation (LPO) of the rock-forming minerals in these granulite mylonites allow a better understanding of deformation mechanisms active at high temperature in the crust. Plagioclase crystals are plastically deformed; they display curved twins and cleavages, mechanical twins, and evidence of dynamic recrystallization. LPO of plagioclase is consistent with activation of the (010) [100] and (010) [001] slip systems. LPO of orthopyroxene and amphibole indicates that these minerals have been deformed through dislocation creep with the activation of the (100) [001] slip system. Quartz in granulite mylonite displays evidence of extensive growth through grain boundary migration. The LPO of quartz is therefore the result of a static transformation of an initial, syn-kinematic LPO, and cannot be straightforwardly interpreted in terms of deformation mechanisms active during mylonitization. © 2002 Published by Elsevier Science B.V.

Keywords: Transpression; Neoproterozoic; Ribeira belt; Lattice preferred orientation

1. Introduction

The Ribeira belt of southeastern Brazil (Fig. 1) formed at the end of the Neoproterozoic Gondwana assembly, along the eastern boundary of an Archean to Neoproterozoic proto-continent that stabilized before 600 Ma. This continental domain involved the São Francisco craton, its eastern rifted margin, and the Neoproterozoic Brasilia belt located to the west and southwest of the craton. Haralyi and Hasui (1982) and Brueckner et al. (2000) have suggested that the eastern limit of this continental domain is underlined by a gravity and magnetic anomaly. According to Pedrosa-Soares et al. (1998), the spatial

* Corresponding author.
E-mail address: megydios@usp.br (M. Egydio-Silva).

0040-1951/02/$ - see front matter © 2002 Published by Elsevier Science B.V.
PII: S0040-1951(02)00197-X

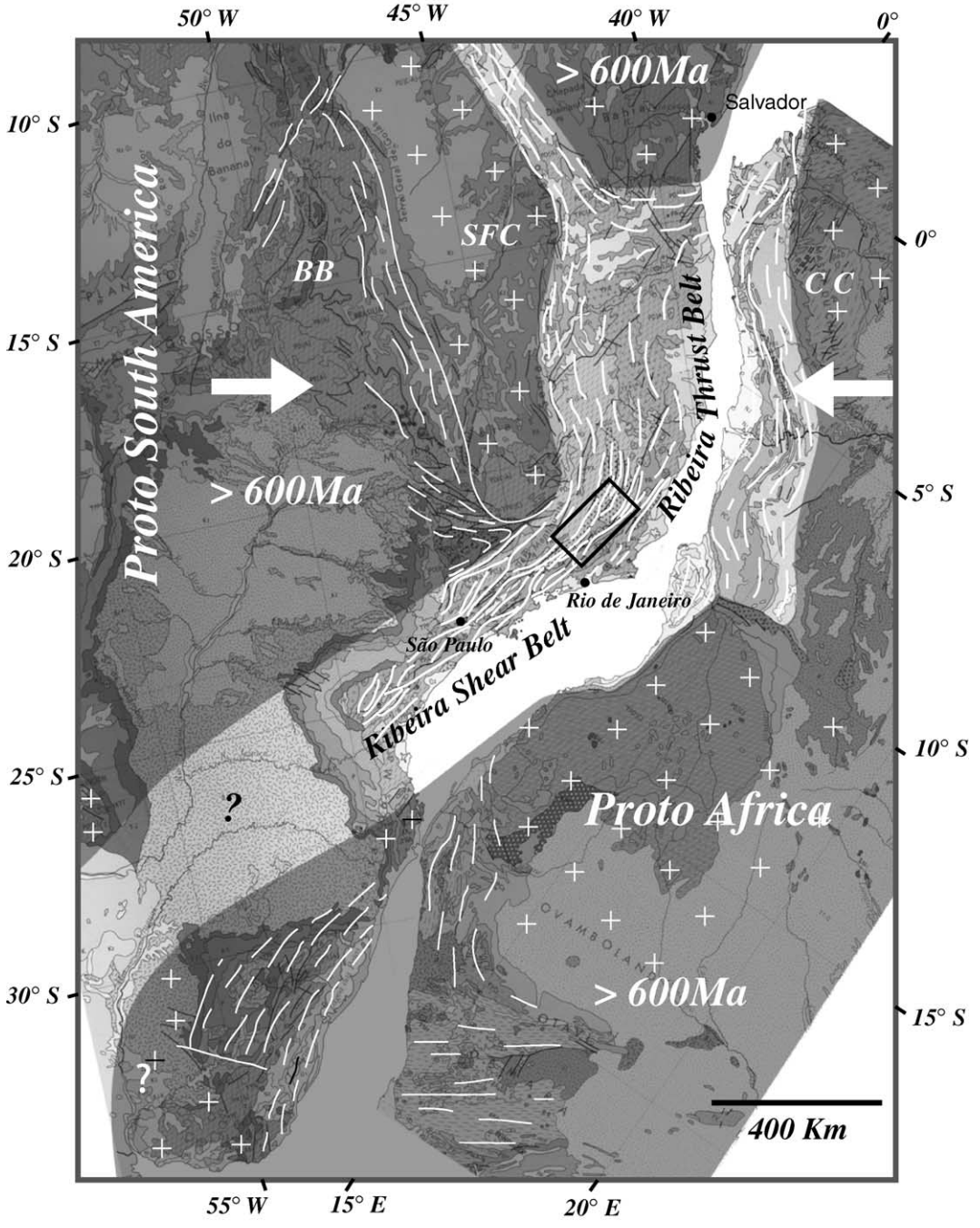

Fig. 1. Cartoon showing the repartition of continental lithosphere stabilized before 600 Ma (proto-South America and proto-Africa, shaded) and after 600 Ma (the Ribeira belt). This highlights the curved shape of the Ribeira belt, and the transpressive character of the southern-domain. SFC = São Francisco craton, CC = Congo craton and BB = Brasilia belt.

association of these anomalies with meta-ultramafic rocks indicates that they may represent the remnant of an ancient oceanic crust. To the east, the Ribeira belt contains abundant igneous rocks of tonalite, granodiorite and diorite composition, and granulites of igneous and metasedimentary origin. This belt may represent a pervasively deformed and metamorphosed magmatic arc. This assemblage suggests a geodynamic scenario involving the closure of a marginal, probably back-arc-basin and the collision of the magmatic arc with the proto-continent at ca. 600 Ma. Evidence of such a tectonic setting is difficult to decipher further south, where the interference between the Ribeira and Brasilia belts and the longitudinal displacements of units along orogen-parallel strike-slip faults make geodynamic interpretations less reliable.

The Ribeira belt displays unusual structural characteristics suggesting that the southern termination of the craton profoundly influenced the strain repartition (Vauchez et al., 1994). The structural trend of the Ribeira belt changes from N020° to the north, along the craton boundary, to N070° southward, beyond the termination of the craton (Fig. 1). This along-strike variation in tectonic pattern correlates with southward variation in syn-kinematic metamorphism, from granulite to amphibolite facies suggesting a variation in erosion level. Vauchez et al. (1994), using finite-element modeling, have suggested that the variation in tectonic style and exhumed metamorphic level along the Ribeira belt results from a lithospheric-scale rheological heterogeneity induced by the termination of the cold and stiff craton. In this model, the northern part of the Ribeira belt was confined westward by the cratonic domain, and this resulted in a thickening of the crust through nappe tectonics. In contrast, to the south of the craton, most of the convergence was accommodated by lateral escape. This model also predicts that the strain regime in the central part of the Ribeira belt should be transpressional, associating lithosphere thickening and belt-parallel strike-slip faulting. Recent isotopic data provide further support to this model since they point toward a broadly synchronous deformation (600–550 Ma) along the Ribeira belt independently of the strain regime (U–Pb and Pb–Pb; Söllner et al., 1991; Machado et al., 1996; Brueckner et al., 2000). Thrusting followed by transcurrent faulting has developed over a short timespan and may be regarded as parts of a single, continuous tectonic evolution.

This paper presents the results of a detailed study of the main transcurrent shear zones of the central Ribeira belt from the regional to the crystal scale. From microstructures and lattice preferred orientation (LPO) analysis, it is shown that the mechanical behavior of the various rock-forming minerals indicates the activation of high-temperature processes, compatible with granulite facies metamorphic conditions. Evidence of transpressional deformation at various scales is also reported. These results allow a discussion of the nature of deformation mechanisms operative in the lower crust, which is still poorly understood.

2. Geological setting

The geology of the eastern and southeastern parts of the Ribeira belt (Fig. 2) is dominated by middle to lower crustal rock sequences, especially migmatitic gneisses and granulites, the protoliths of which have been dated at 2220 ± 27 Ma (U–Pb; Söllner et al., 1991). These rocks have subsequently undergone tectonic, magmatic and metamorphic processes during the Neoproterozoic Pan-African/Brasiliano orogeny, ($\sim$ 600–520 Ma). The northern part of the belt is characterized by two different rock sequences: the Paraíba do Sul and Juiz de Fora complexes. The former contains kinzigites, garnet–biotite–plagioclase gneisses, migmatites and granulite gneisses, whereas the latter complex is dominated by granulitic gneisses of enderbitic and mangeritic compositions and basic granulites. Charnockites free of solid-state deformation are observed in both domains. U–Pb radiometric age determinations highlight an evolution from 2200 to 500 Ma ago (Machado et al., 1996). The oldest ages obtained for high-grade gneisses from the Juiz de Fora and Paraíba do Sul complexes are in the range 2185–2134 Ma. They have been related to the Transamazonian orogeny (Machado et al., 1996), the earliest thermo-tectonic event in the region. Subsequently, these rocks have been affected by the Pan-African/Brasiliano event ($\sim$ 600–520 Ma).

In the studied area, two principal deformation events, belonging to a Neoproterozoic orogeny, have been documented. Early thrusting to the WNW started

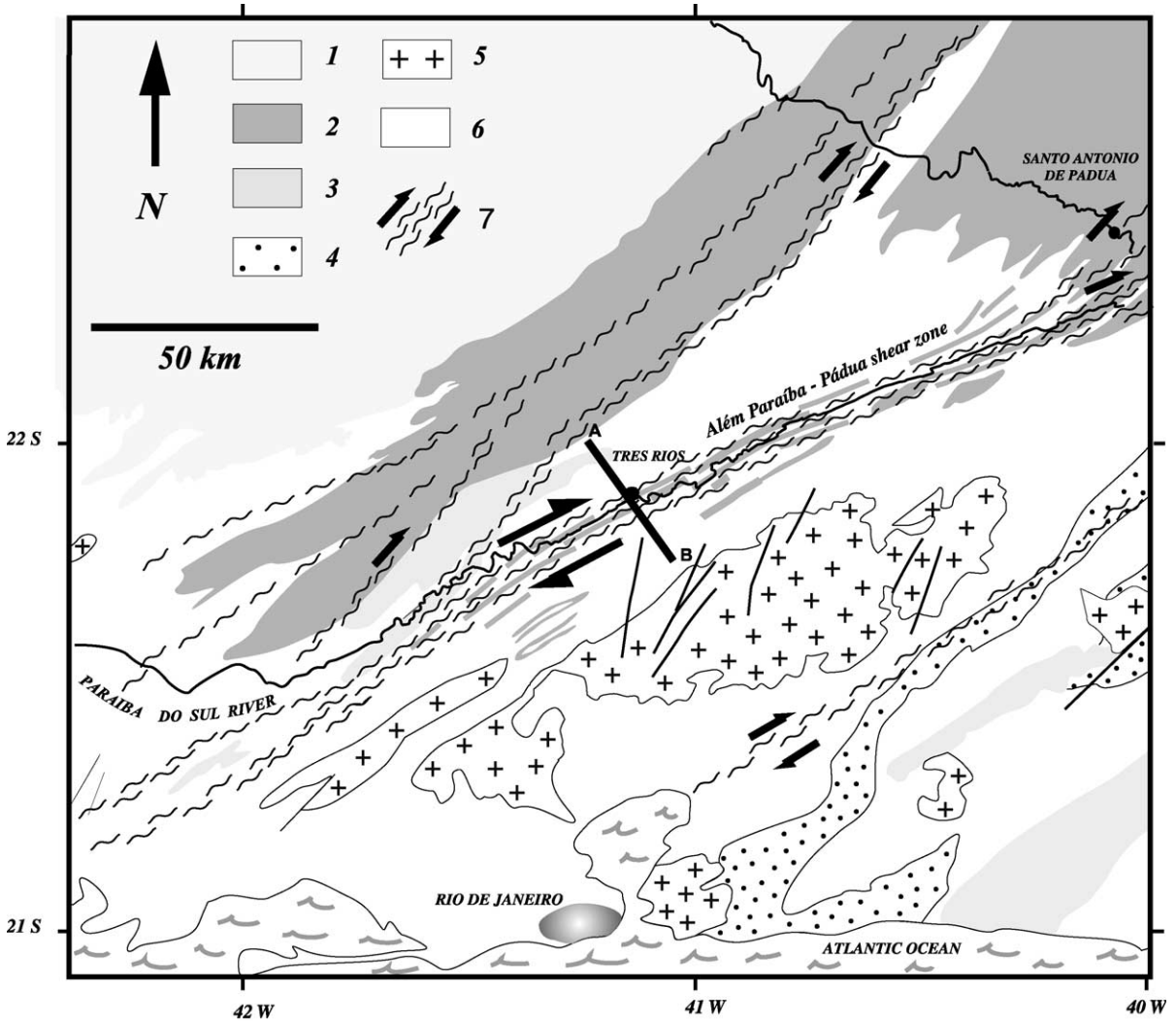

Fig. 2. Schematic geologic map of the Além Paraíba–Pádua shear zone. (1) Polycyclic basement, (2) Juiz de Fora complex, (3) enderbite, (4) kinzigite, (5) syntectonic granites, (6) Paraiba do Sul complex, (7) mylonitic rocks.

before 589 ± 8 Ma (monazite and titanite ages), and was followed by slightly younger dextral transcurrent shearing that occurred before 535–527 Ma (zircon, monazite and titanite U–Pb ages; Machado et al., 1996). A continuous metamorphic evolution involving two metamorphic episodes, both in the granulite facies, has been suggested by Porcher (1997). The first event occurred under temperature conditions of ca. 850 °C and pressures between 600 and 670 MPa in the southern area (Três Rios–Rio de Janeiro state), and from 810 to 880 °C in the north (Santo Antônio de Pádua–Rio de Janeiro state). This metamorphic episode is preserved in granulites that have escaped the transcurrent deformation and have retained a low-angle foliation defined by the alignment of hypersthene, plagioclase, quartz, biotite, garnet and clinopyroxene. According to Machado et al. (1996), the peak metamorphism was reached between 589 and 563 Ma (monazite and titanite ages). A slightly lower-grade metamorphic imprint was recorded during the development of the transcurrent shear zones before 535–527 Ma (Machado et al., 1996). PT conditions

evaluated from chemical analysis range from 715 to 747 °C and 450 MPa for the southern area, and from 734 to 743 °C and 520 MPa for the northern area (Porcher, 1997).

Hypersthene is the diagnostic mineral in these rocks, most of which are quartz–feldsphatic granulitic gneisses with plagioclase, quartz, and/or perthitic alkali–feldspar, hypersthene, biotite and garnet. Sillimanite is sometimes present, especially in kinzigitic gneisses, associated with garnet, hornblende, biotite and plagioclase. Gneisses with mineral assemblages involving clinopyroxene, garnet, hornblende, and biotite are also observed in close association with the kinzigitic gneisses. Similar assemblages that are free of biotite have been observed locally, suggesting that during the early stage of deformation dry granulites have been formed.

In summary, tectonic and metamorphic evidence hints to a continuous evolution in which thrusting and transcurrent faulting under high temperature and relatively low pressure were associated. This evolution is likely related to the progressive closure of an arcuate residual basin between the eastern and western Gondwana protocontinents during a period of time that straddles the upper Neoproterozoic–Cambrian boundary.

3. Além Paraíba–Pádua shear zone system

The Além Paraíba–Pádua shear zone system (APPSS) represents the northern termination of a network of ductile strike-slip shear zones that extends for over 1000 km in the southern Ribeira belt. It involves dextral transcurrent shear zones oriented N070° and N040° in the southern and northern portions, respectively (Figs. 1 and 2). These shear zones are characterized by a mylonitic foliation developed under high-temperature/low-pressure conditions in the middle/lower crust. In the Pádua area, several zones of granulitic mylonites form a network parallel to the general trend of the belt. The Além Paraíba shear zone is slightly oblique to the tectonic grain of the belt and to the Pádua network, and may be regarded as a mega C' shear band, i.e., a strain transfer zone within the belt that accommodated the orthogonal component of contraction in a transpressional system. The deformation pattern of this region, as reported above, was likely controlled by the rheological heterogeneity of the lithosphere in the area, especially that introduced by the southern termination of the São Francisco craton (Figs. 1 and 2; Vauchez et al., 1994).

High-temperature mylonites in the shear zones have both igneous and sedimentary protoliths. They are granulites of noritic composition, kinzigitic gneisses, amphibolites, gabbroic gneisses and some plagioclase-rich migmatites. To the north, mylonites equilibrated under granulite facies conditions are predominant in both the Além Paraíba and the Pádua shear zones. To the south, granulitic mylonites outcrop as lenses a few hundred metres to a few kilometres of extension embedded in migmatitic gneisses, frequently hornblende bearing, that still preserve few pyroxenes. This suggests that the granulitic mylonites remained metastable during late stages of deformation coeval with cooling down to the upper amphibolite facies conditions. A common characteristic of the various types of mylonites is that, when compared to their host rocks, they do not show any grain-size reduction.

The mylonitic foliation trends predominantly NE–SW in the Pádua system and ENE–WSW in the Além Paraíba shear zone. On both sides of the Além Paraíba shear zone, the dip of the foliation decreases to the SE and NW in a fan-like configuration (Fig. 3). Such a

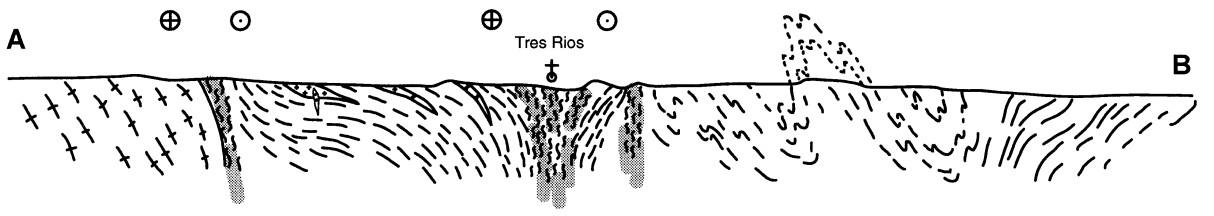

Fig. 3. Schematic cross section (A–B) along the Além Paraíba–Pádua shear system.

configuration is not observed in the Pádua system where the foliation consistently dips steeply to the SE. The mylonitic foliation contains a ubiquitous mineral stretching lineation (Fig. 4), which is gently southward plunging in the Pádua shear zone and subhorizontal in the Além Paraíba shear zone. Stretching is marked by boudinage of the foliation or of the more competent layers, shape preferred orientation of sillimanite prisms, amphibole, biotite and oxides (especially ilmenite), elongate recrystallized tails around porphyroclasts, and ductilely elongated plagioclase crystals.

Kinematic indicators in the granulite facies mylonite are scarce. This is probably due to a combination of pure and simple shear components in a transpressional deformation that tends to impede the development of asymmetrical structures (e.g., Vauchez et al., 1995), and to extensive annealing of mylonites. The most common kinematic indicators are asymmetrical tails of dynamically recrystallized feldspar on porphyroclasts. σ-type porphyroclasts (Passchier et al., 1992) are more commonly observed, but δ-type have been occasionally found (Fig. 5A). Stiff layers of amphibolites embedded in more felsic mylonites display rotated asymmetric boudins (Fig. 5B). Locally, shear bands have been observed. In any case, mesoscopic and microscopic kinematic indicators in the APPSS consistently suggest a dextral sense of shear.

4. Microstructure, deformation mechanisms and LPO development in the shear zones

Rock-forming minerals are largely segregated into elongate, almost monomineralic layers or ribbons that define the foliation (Fig. 6A). The ribbons wrap around porphyroclasts that may be remnants of parent plagioclase, garnet, orthopyroxene and/or clinopyroxene grains. At the grain scale, those mylonites display microstructures typical of high-temperature conditions prevailing during and after ductile deformation. Syn- to post-kinematic annealing is supported by evidence of efficient diffusion (recovery, pervasive grain boundary migration and grain growth, static recrystallization). This is in good agreement with thermobarometric determinations and mineral assemblages, and raises the question of whether the LPO of the main minerals observed in granulitic mylonites (quartz, plagioclase, pyroxene and amphibole) is representative of syn-kinematic processes or has been deeply affected by post-kinematic (static) evolution.

5. Lattice preferred orientation measurement technique

Determinations of LPO of quartz, plagioclase, hypersthene and amphibole were made with a scan-

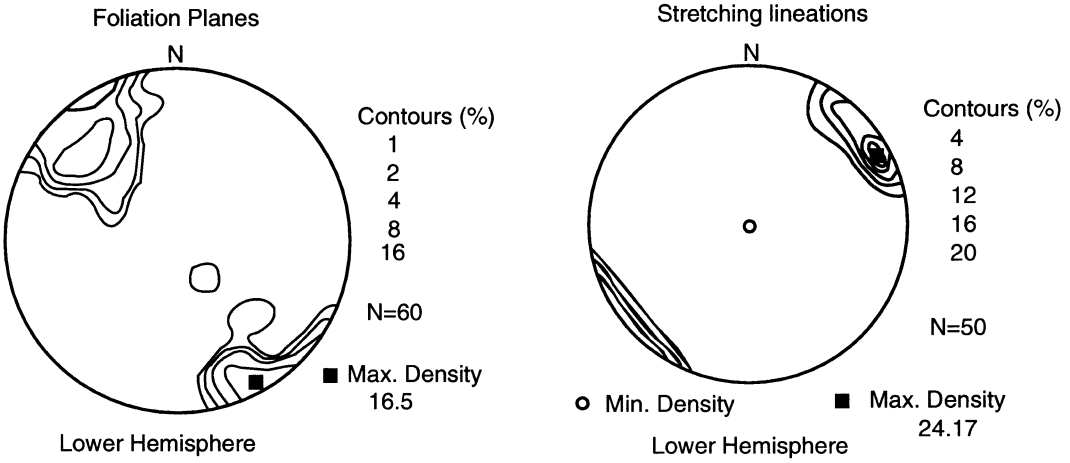

Fig. 4. Foliation and lineation orientations in the Além Paraíba–Pádua shear system.

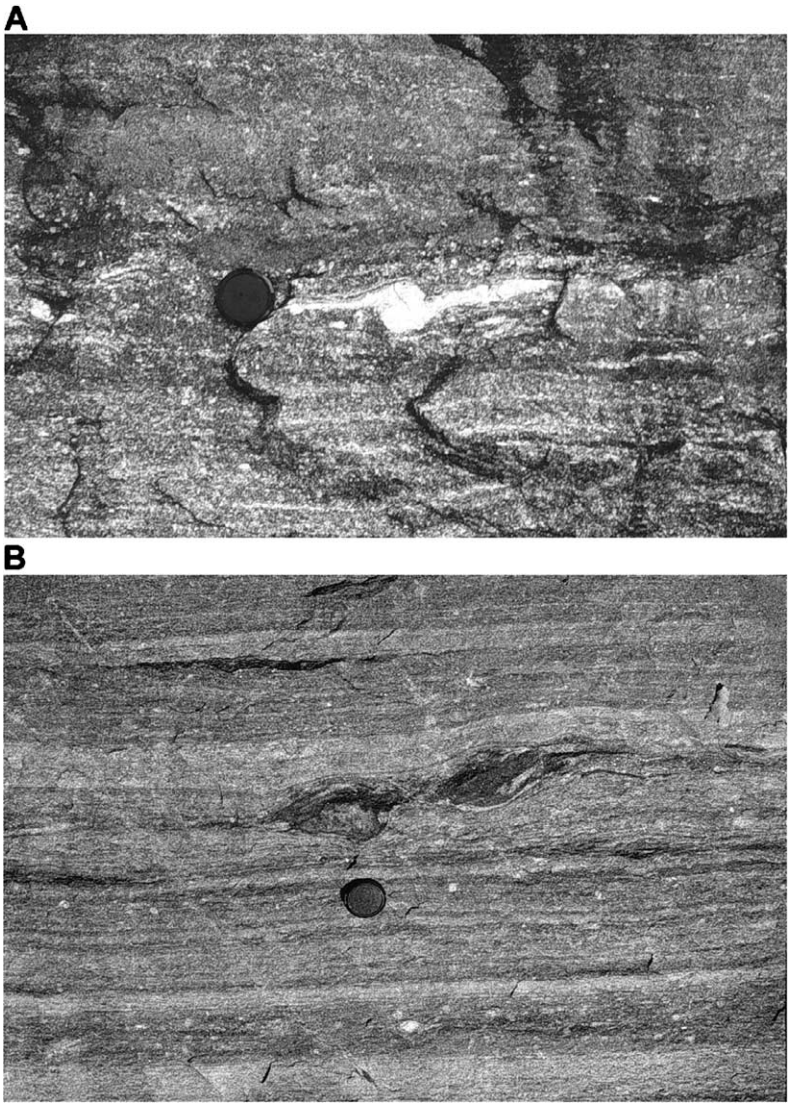

Fig. 5. (A) Dextrally rotated δ-type winged feldspar porphyroclast in mylonite granulite. (B) Dextrally rotated amphibolite inclusions inside Além Paraíba shear zone.

ning electron microscope JEOL JSM 5600 (Laboratoire de Tectonophysique, University of Montpellier) through the indexation of electron back-scattered diffraction patterns (EBSD; Lloyd et al., 1991; Adams et al., 1993; Dingley and Field, 1997). Diffraction patterns have been generated by the interaction of a vertical electron beam with a crystal in an ultra-polished thin section tilted 70° relative to the horizontal plane, then projected onto a phosphor screen. A low-light, high-resolution digital camera records the photonic image of the diffraction pattern, which is then processed and indexed using the CHANNEL+ software from HKL Technology (Schmidt and Olesen, 1989). The nature of the mineral and the Euler angles ($\varphi 1$, ϕ, $\varphi 2$) characterizing the lattice orientation are stored for each measurement. The whole procedure (pattern acquisition, image freezing, kikuchi bands detection, indexing and result backup) can be carried out automatically, however, in this work the lattice preferred orientation

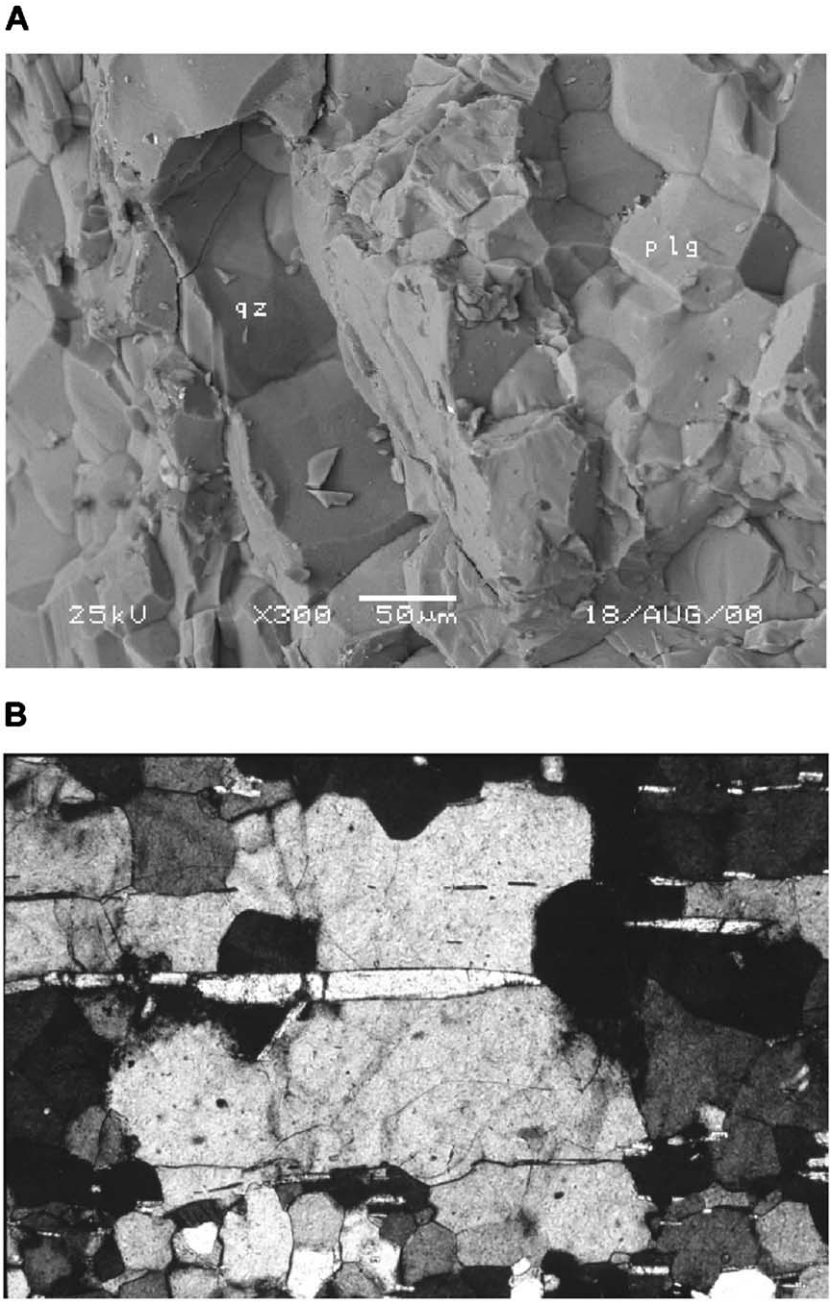

Fig. 6. (A) SEM photomicrograph of gneiss composed of alternating layers of recrystallized feldspars (plg) and quartz (qz) ribbons. (B) Optical photomicrograph of quartzite mylonite showing sillimanite crystals parallel to the foliation.

has been measured grain-per-grain and diffraction patterns have been visually inspected before recording the results. In complement, LPO of quartz and plagioclase in a few samples were measured previously using a five-axes universal stage at São Paulo University.

6. Quartz: annealing fabric

Quartz in granulitic mylonites displays a limited variety of microstructures. When the modal proportion of quartz is high enough, quartz is segregated into almost monomineralic ribbons interlayered with other mineral components. Four main quartz LPO types have been observed, they are associated with contrasting microstructures and may represent various degrees of combination between syn- and post-kinematic processes.

The most common type displays a tabular shape and a large grain size (platten-quartz type). Usually, platten-quartz ribbons are made of a single layer of crystals. The individual grains have straight or slightly curved boundaries with dihedral angles close to 90°. Most grains do not display any substructure; in those grains that do, the microstructure is restricted to a weak undulose extinction and rare sub-boundaries. These grains frequently contain inclusions of elongate plagioclase, micas or prismatic sillimanite aligned parallel to the mylonitic foliation (Fig. 6B).

Tabular quartz ribbons display a LPO characterized by a maximum of [0001] axes close to the *Y* tectonic direction, and the absence of subsidiary maximum close to *Z* or *X* (*X*: lineation direction; *Z*: normal to the *XY* foliation plane). The concentration of the *c*-axis around *Y* is either isotropic, resulting in an almost circular shape of the contours, or slightly elongated between the *Y* and *Z* directions defining a short girdle in the *YZ* plane (Fig. 7C). The ⟨*a*⟩ and ⟨*m*⟩ axes have a maximum density that is close to the stretching lineation (Fig. 7A and B). This type of LPO is common in high-temperature mylonites and is interpreted to result from activation of the prism ⟨*a*⟩ slip system (Nicolas and Poirier, 1976; Bunge and Wenk, 1977; Starkey, 1979; Schmid and Casey, 1986).

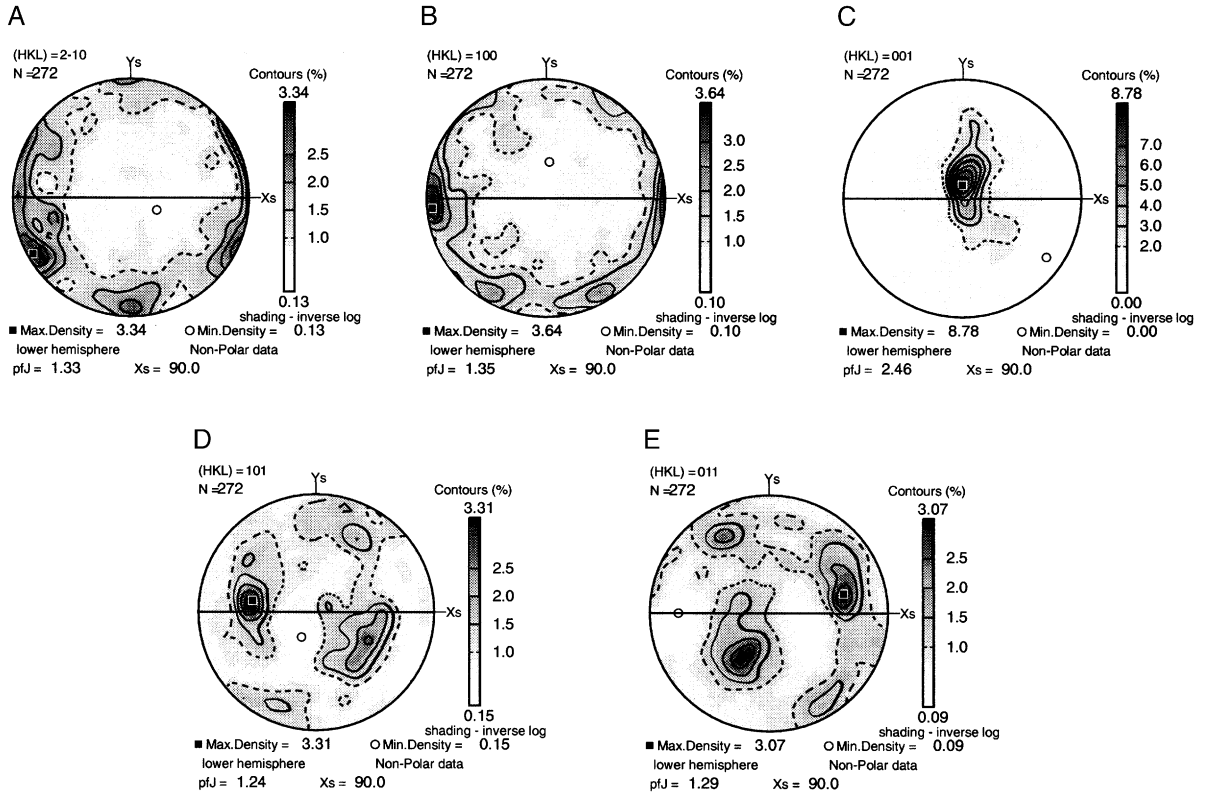

Fig. 7. Statistical distribution in equal area diagrams of the complete quartz fabrics (sample RB614).

A second quartz *c*-axis orientation pattern was observed in a mylonitic granodiorite gneiss, showing deformed and recrystallized plagioclase grains (55–60%), recrystallized polygonal quartz grains (20–25%) and some K-feldspar and biotite. This fabric is associated with a microstructure characterized by polygonal quartz grains, many of them five- or six-sided, exhibiting straight boundaries meeting at triple junctions. Quartz also forms monomineralic polycrystalline ribbons but there are some grains within the feldspar-rich domains. The *c*-axis pole figures (Fig. 8) display a single girdle skeleton with two maxima on the *ZY* plane of the structural framework, asymmetrically (RB70, Fig. 8C) or symmetrically (RB523, Fig. 10B) distributed with respect to the mylonitic foliation plane. Complete LPOs shown on Fig. 8A and B displays ⟨*a*⟩ and ⟨*m*⟩ axis patterns similar to those of sample RB614 (Fig. 7A and B), i.e., with a density maximum near the stretching lineation. The ⟨*r*⟩ and ⟨*z*⟩ axes display a poorly organized pattern.

The third type of quartz LPO is characterized by two maxima of *c*-axis orientations symmetrically located between the *Y* and *Z* structural axes (Fig. 10C). The maximum concentration is high and no significant subsidiary maxima exist. This crystallographic fabric was observed in mylonites in which quartz grains are equidimensional, usually smaller in size than the platten-quartz (a few hundred micrometres), and display straight boundaries with dihedral angles of about 120°. These crystals are free of any substructure, and contain inclusions of other minerals aligned parallel to the mylonitic foliation (Fig. 6B). Tabular and equidimensional grains may coexist and

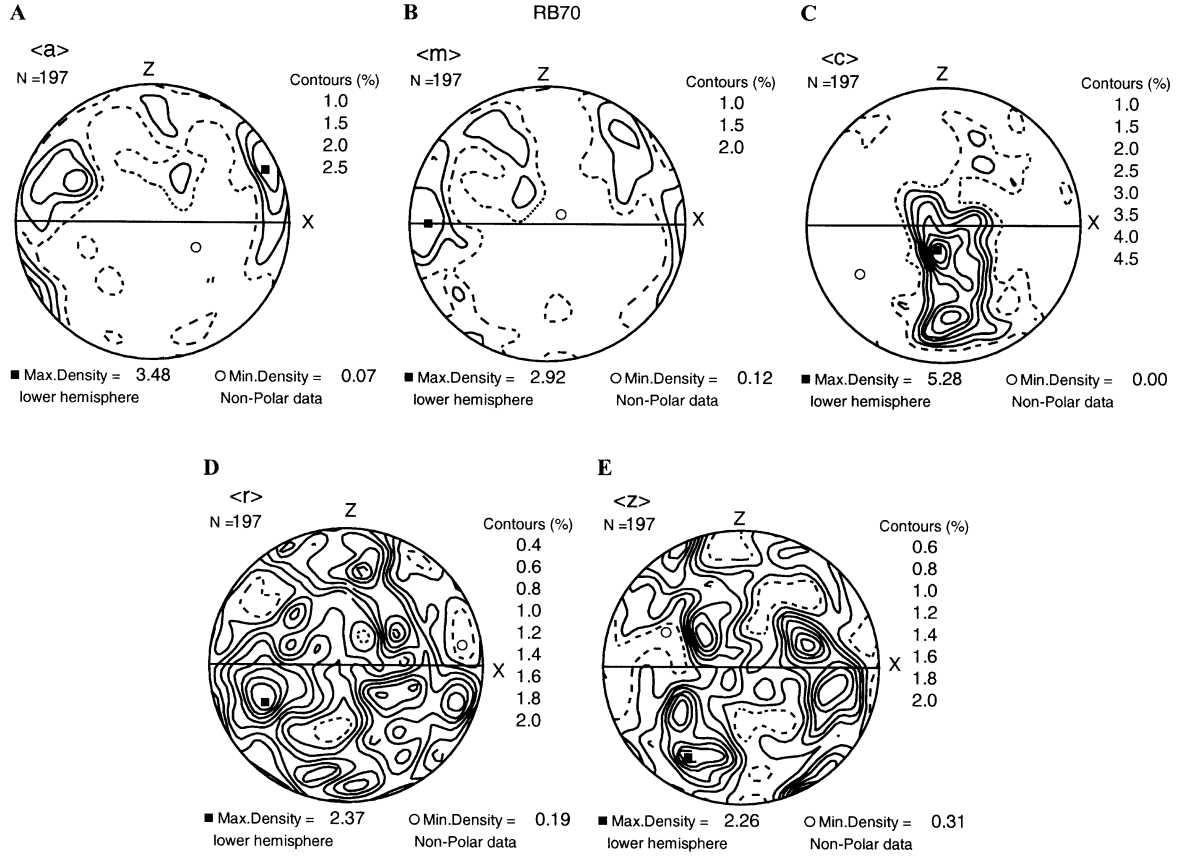

Fig. 8. Isofrequency curves in equal are diagrams for the complete quartz fabric (sample RB70).

in a few cases, evidence for a transition from tabular to equidimensional shapes has been observed. In these specimens, equidimensional grains surround larger tabular crystals. The contact between the two types is usually complex, small polygonal grains being frequently enclosed by a larger one. As a result, grain boundaries of large quartz crystals are extremely irregular, they display reentrants and promontories made of small straight segments giving a typical faceted aspect to the larger crystals. The proportion of small and large grains is variable from sample to sample and in some cases, original grains only subsist as skeletal minerals within a matrix of finer, equant polygonal grains (Fig. 14A).

The fourth type of quartz LPO has been observed in an intensely deformed mylonite. The main characteristic of this mylonitic gneiss is that almost all the quartz content of the rock is concentrated in ribbons, which are separated by feldspar-rich domains that lack quartz. Substructures such as sub-grains and undulose extinction are scarce, and the grains, 60–100 μm in size, show a brick-like shape (Fig. 6A). The respective quartz LPO exhibits a *c*-axis single girdle with a shallowly plunging point maximum that makes a ~ 25° clockwise angle to the pole of the foliation (*Z* axes). This relationship is consistent with the macroscopic sense of the shear (Fig. 9C). The *a*-axis orientation patterns have a tendency to spread along a great circle (Fig. 9A). There is a clustering of *a*-axes at an angle of ca. 25° to the *X* direction. The poles to rhomb crystallographic planes are arranged along two perpendicular planes (~ N–S and E–W) with a maximum density near *Z* (Fig. 9D). The preferred orientation of the first order prisms {*m*} and the *a*-axis patterns are similar, but the distribution of the normal to the rhomb planes is more diffuse (Fig. 9E). Helming et al. (1994) have suggested that ⟨*m*⟩ preferentially oriented sub-parallel to the lineation could be generated by recrystallization (Fig. 9B).

These four main types of quartz LPO are not randomly distributed. Types 1 and 2 (Fig. 10A and B) are typical of mylonites at the boundaries of the

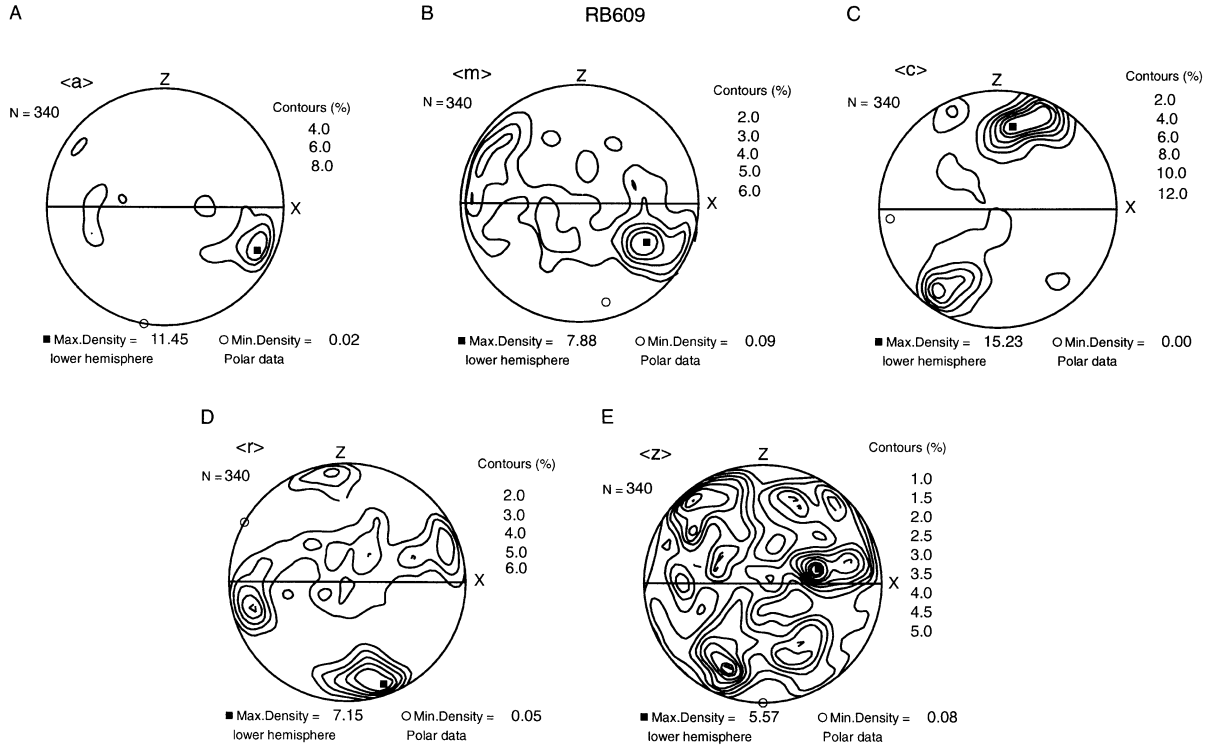

Fig. 9. Pole figures in equal area diagrams of the *c*-axis (C) second-order prisms (A), first order prisms (B), positive rhombs (D) and negative rhombs (E) (sample RB609).

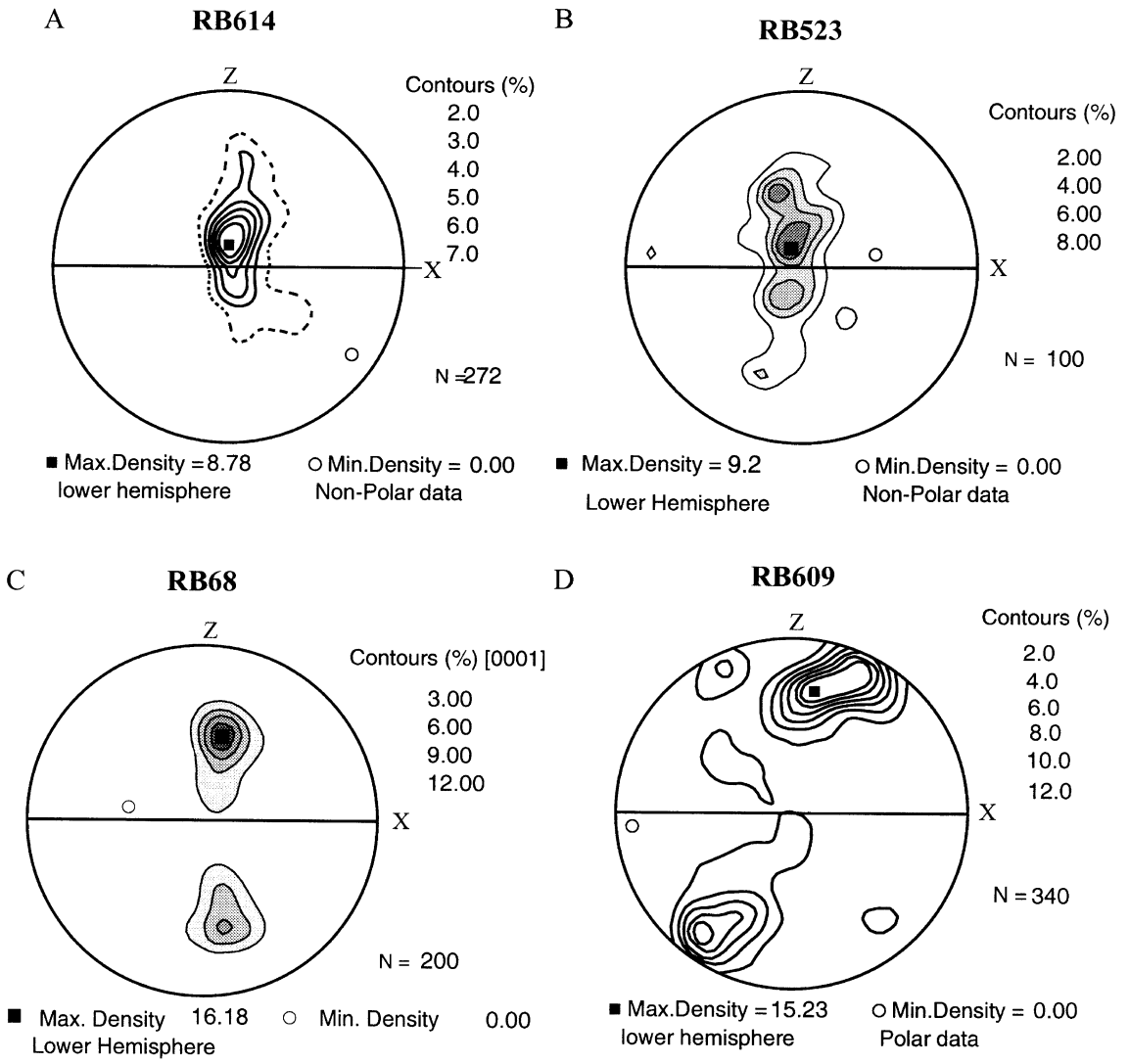

Fig. 10. *c*-Axis fabrics of samples from moderate- to high-strain domains of the mylonite shear zone. Fabrics are ordered by increasing deformation intensity.

shear zones. Types 3 and 4 (Fig. 10C and D) have been observed in mylonites in the core of the shear zones.

7. Quartz LPO discussion

Granulitic mylonites consistently display evidence of syn-tectonic recrystallization under high-temperature conditions and static evolution of their microstructure due to annealing (for a general discussion of the processes and their effects in crystalline materials see Humphreys and Hatherly, 1995). During annealing, the microstructure of the polycrystalline material continued to evolve at high temperature even after the differential stress was removed because diffusion continued to operate. The main recrystallization mechanism involved is grain boundary migration, which can generate two different types of recrystallized grains. Limited annealing leads to recovery

through the formation of strain-free new grains with straight boundaries that meet at angles of 120° (triple-grain junctions). More severe annealing results in extensive grain growth through the consumption of grains having a higher dislocation density (higher stored energy). When quartz grain size is bimodal, lower surface energy may also favor growth of coarser crystals and consumption of the finer ones providing their stored energy is similar. In rocks where strain-induced segregation led to compositional layering, grain boundary migration normal to the foliation is limited and grain growth results in the development of platten-quartz. In quartz-rich rocks, grain boundary migration is less dimensionally constrained. Extensive grain boundary migration results in the inclusion of small, pre-existing crystals in large quartz grains (Fig. 6B).

The significance of quartz LPO in rocks that have undergone extensive annealing is still poorly understood. The extent of the modification of the initial LPO by static recrystallization is poorly constrained. On one hand, where grain boundary migration was restricted to the polygonization of crystals without significant growth, the syn-kinematic LPO was probably not totally erased. On the other hand, where extensive grain growth deeply modified the microstructure, it may have also modified the LPO pattern and symmetry. Experiments by Hobbs (1968), Green et al. (1970) and Masuda et al. (1997) were not conclusive in this regard. More recently, Heillbronner and Tullis (2001) have reported results from experimentally annealed quartzite showing that the pre-existing LPO of quartz was largely preserved although the size and shape of crystal is significantly modified. However, these results do not account for the peculiar LPO observed in extensively annealed quartz-rich mylonites as those within the Além Paraíba–Pádua shear system. These LPO (types 3 and 4 especially) cannot be explained by the activation of one or several high-temperature (prismatic) slip systems identified in quartz deformed under granulitic conditions (e.g., Nicolas and Poirier, 1976; Mainprice et al., 1986). Consequently, the LPO of quartz in extensively annealed mylonites cannot be merely interpreted in terms of active slip systems and kinematics. These LPO may have been largely modified by post-tectonic diffusion through a selection process favoring some of the initial crystallographic orientations at the expenses of the others.

The transition from types 1 and 2 to types 3 and 4 of quartz LPO from the periphery to the center of the shear zones might reflect either a difference in the syn-kinematic LPO or contrasting post-kinematic evolution of the LPO, possibly in relation to a thermal gradient. Considering that mylonitization in the Além Paraíba–Pádua shear zone system occurred under HT-LP conditions (≥ 800 °C; 600–700 MPa), a possible source for LPO variations might be an effect of the $\alpha-\beta$ quartz transition either during mylonitization or during post-kinematic annealing (e.g., Green et al., 1970). Indeed, the exaggerated growth of quartz in most studied mylonites is also in agreement with an evolution in the β-quartz stability field. LPO variation across small-scale shear zones formed under amphibolite facies conditions was already described by Vauchez (1987) who tentatively suggested that either variations in temperature or in water content may have favored a switch in the dominant slip system.

8. Plagioclase

Granulitic mylonites display alternating quartz- and plagioclase-rich layers. The plagioclase-rich domains resulted from the dynamic recrystallization of porphyroclasts and as a result, only a few porphyroclasts are usually preserved. These porphyroclasts are plastically deformed and frequently display mechanical twins, bent cleavage and twin planes, sub-boundaries and sub-grains. Recrystallized plagioclase grains are from 30 to 150 μm in size and are strain-free; they are usually almost equidimensional and display a polygonal shape with 120° dihedral angles (Fig. 11A). Some recrystallized grains show evidence of heterogeneous grain boundary migration (Fig. 11B) due to heterogeneous grain boundary migration. The overall microstructure of plagioclase suggests a deformation accommodated through an association of dislocation creep, dynamic recrystallization and limited grain boundary migration (diffusion).

Ji and Mainprice (1990) and Egydio-Silva and Mainprice (1999) have shown that there is no significant difference between the crystallographic fabric of recrystallized and porphyroclastic plagioclase grains. In this study, the LPO of the recrystallized and relic plagioclase grains have been indistinctly measured.

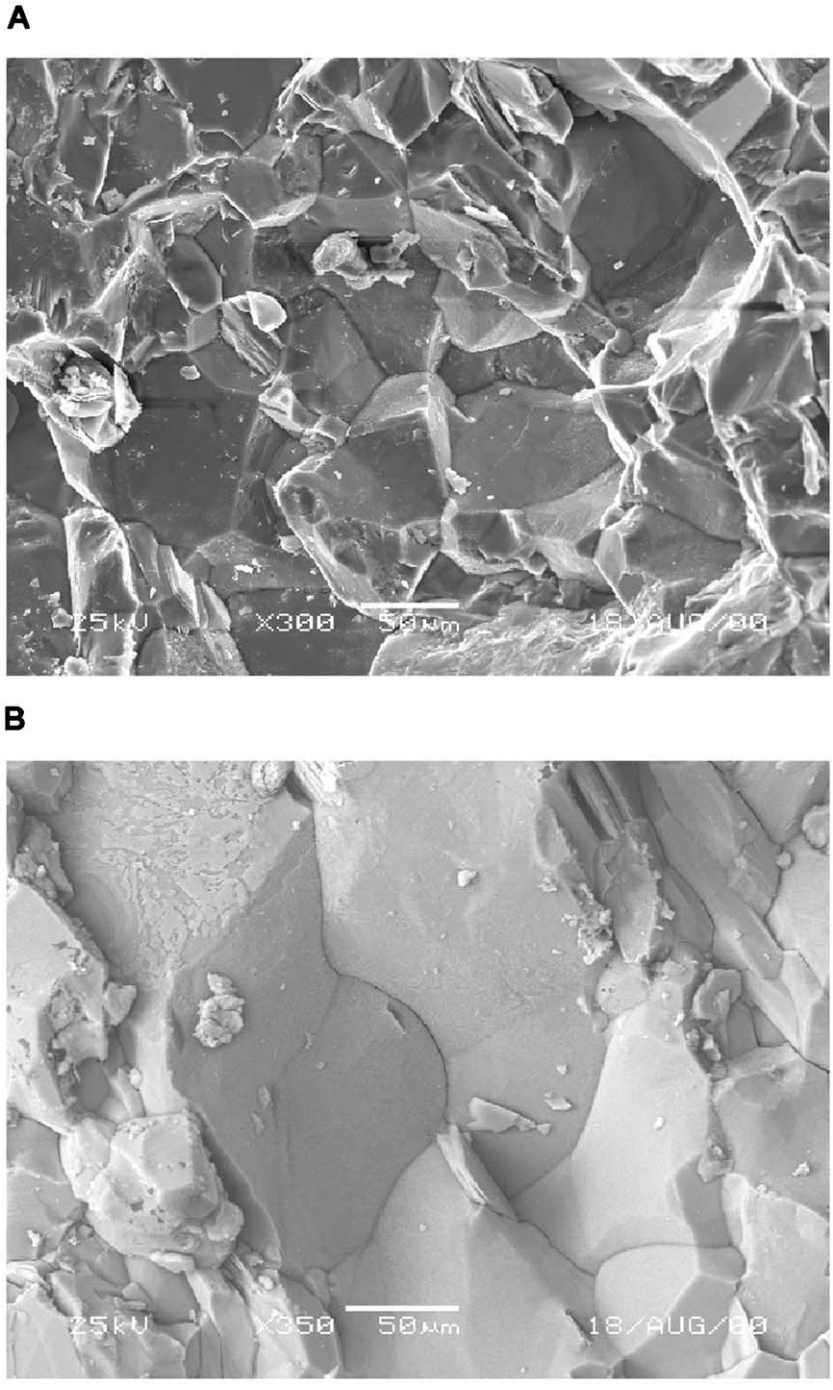

Fig. 11. (A) Recrystallized plagioclase grains with polygonal shapes. Straight grain boundary configurations meet at 120° triple junctions. (B) Grain boundary migration microstructure in deformed feldspar from central Além Paraíba–Pádua shear system.

LPO of the samples RB5, RB70 and RB95 is shown in Fig. 12. In general, the (010) poles concentrations display two maxima, a stronger one close to the foliation pole (Fig. 12B, E and H) and a subsidiary maximum sub-parallel to the stretching lineation (Fig. 12H). The [100] axes are preferentially oriented sub-parallel to the *Y* structural direction (Fig. 12A, D and G), whereas the orientation pattern of the (001) poles is more complex and diffuse (Fig. 12C and F). In the same samples (RB559, RB540 and, RB609A), the [100] axes form a girdle parallel to the foliation plane with a maximum near *Y* (Fig. 13A). In the remaining samples (Fig. 13D and G), [100] shows a more complex pattern. The (010) poles form a maximum that is approximately perpendicular to the foliation plane, and the asymmetry of this maximum concen-

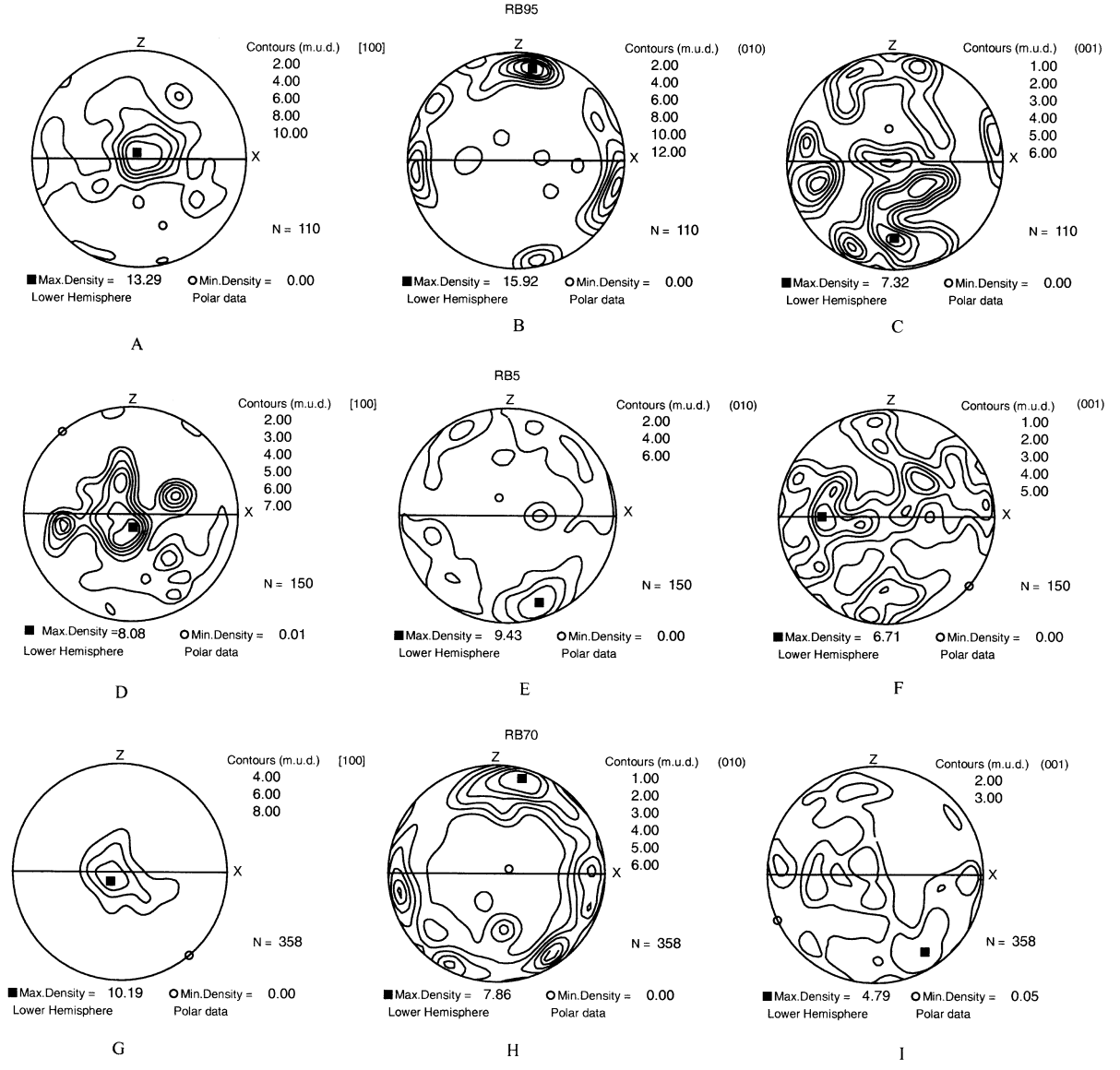

Fig. 12. Preferred orientation of plagioclase crystallographic axes in the gneiss mylonite from the Além Paraíba–Pádua shear system (samples RB95, RB5 and RB70).

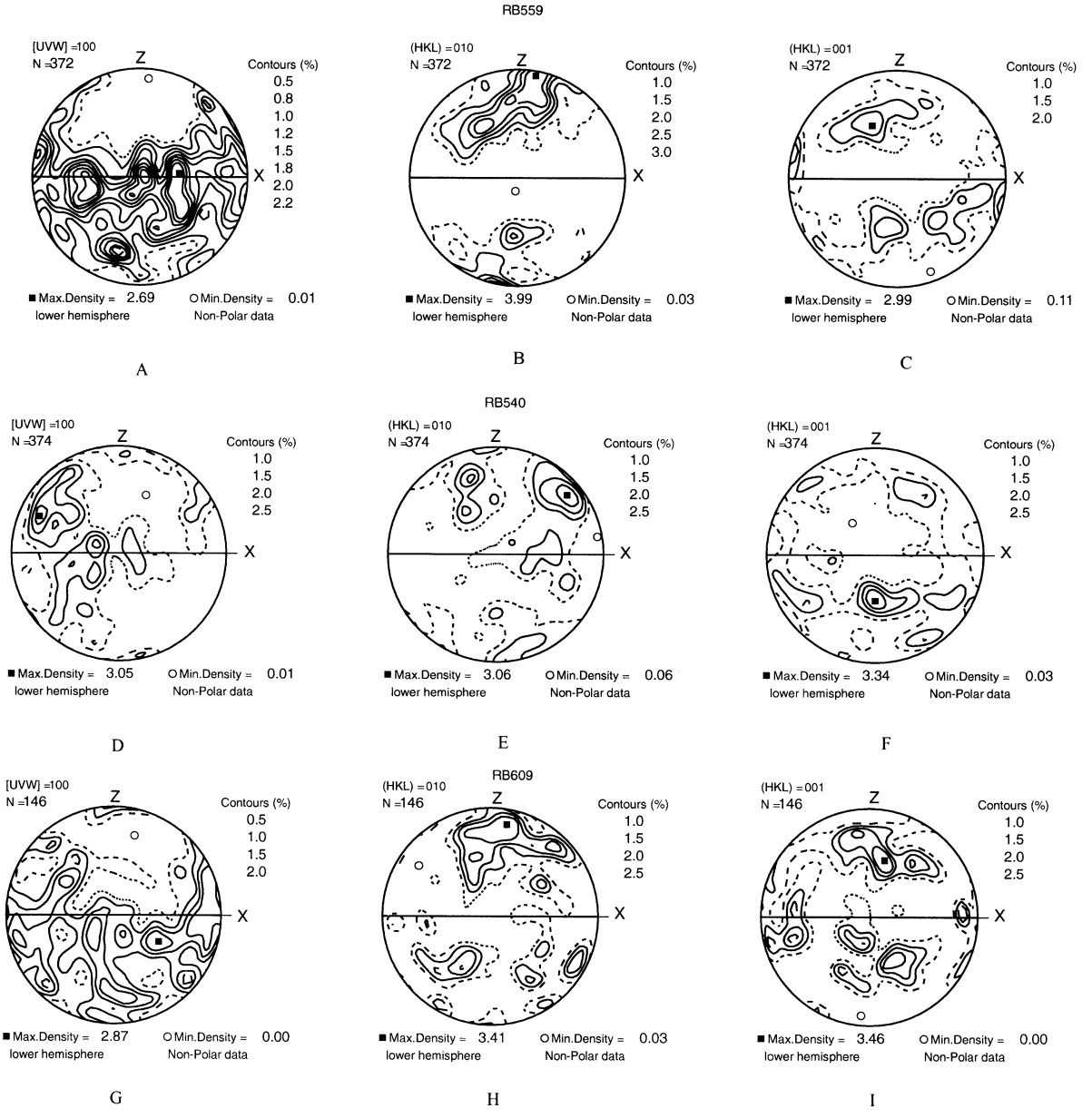

Fig. 13. Preferred orientation of plagioclase crystallographic axes in the gneiss mylonite from the Além Paraíba–Pádua shear system (samples RB559, RB540 and RB609).

tration with respect to the foliation are consistent with a dextral sense of shear (Fig. 13B, E and H). The (001) poles orientation pattern is always difficult to interpret, but there is a tendency for the data to spread along two small circles symmetrically located with respect to the foliation plane (Fig. 13C). The other patterns are more diffuse and complex (Fig. 13F and I).

Orientation of the (010) planes sub-parallel to the foliation plane and of the [100] and [001] axes nearly

parallel to *Y* and *X*, respectively provide indirect evidence for dislocation glide on the (010) [100] and (010) [001] slip systems. This interpretation is supported by TEM observations reported by Olsen and Kohlstedt (1984) and Ji and Mainprice (1988). These authors observed that the highest density of

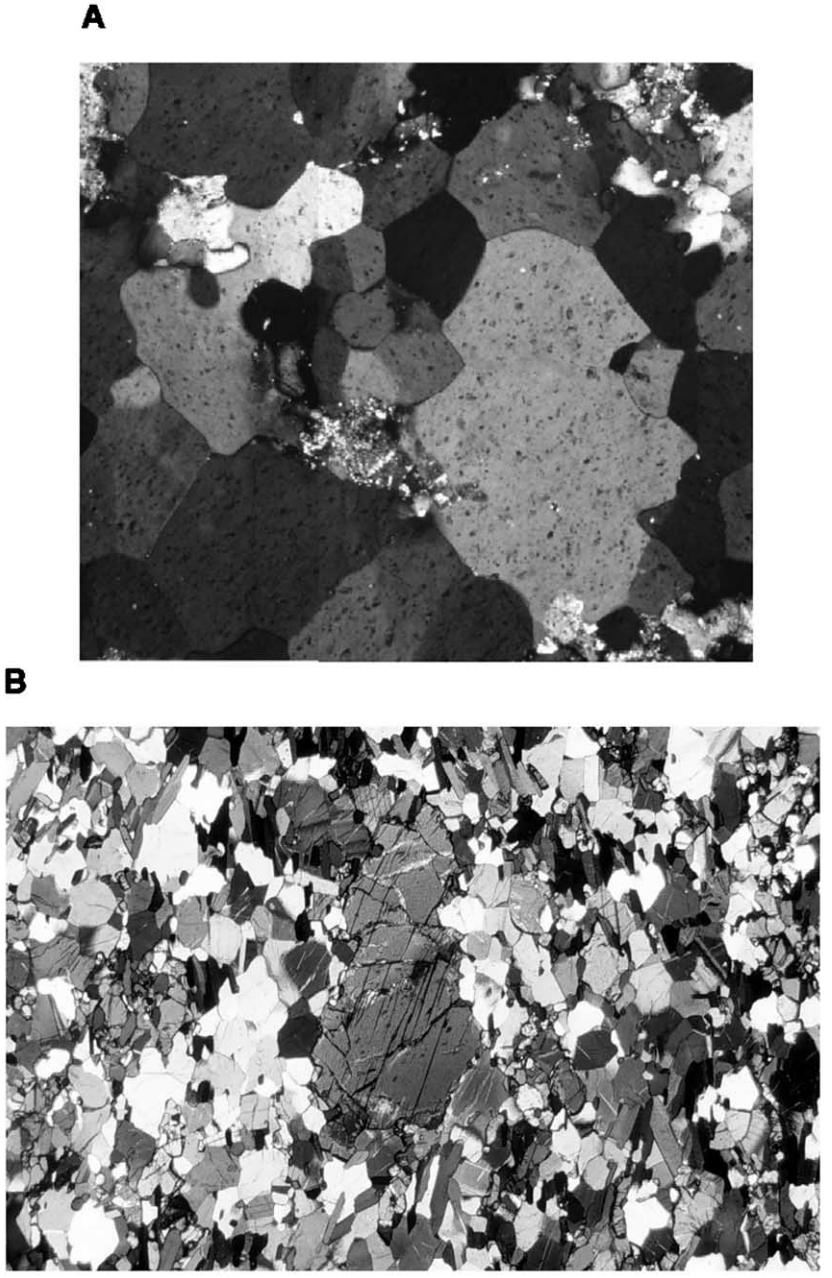

Fig. 14. (A) Photomicrograph of a quartzite mylonite. Quartz grains are recrystallized and show polygonal shapes and evidences of grain boundary migration. (B) Orthopyroxene porphyroclast showing bent cleavage planes.

dislocations was on the (010) planes and that these dislocations were representative of the (010) [001] and (010) [100] slip systems. From these observations, they concluded that, at high temperature, dislocation glide on these slip systems represents the main mechanism for LPO development in plagioclase. LPO observed in the Além Paraíba shear zone is consistent with plastic deformation of plagioclase under high-temperature granulite facies conditions observed in the area.

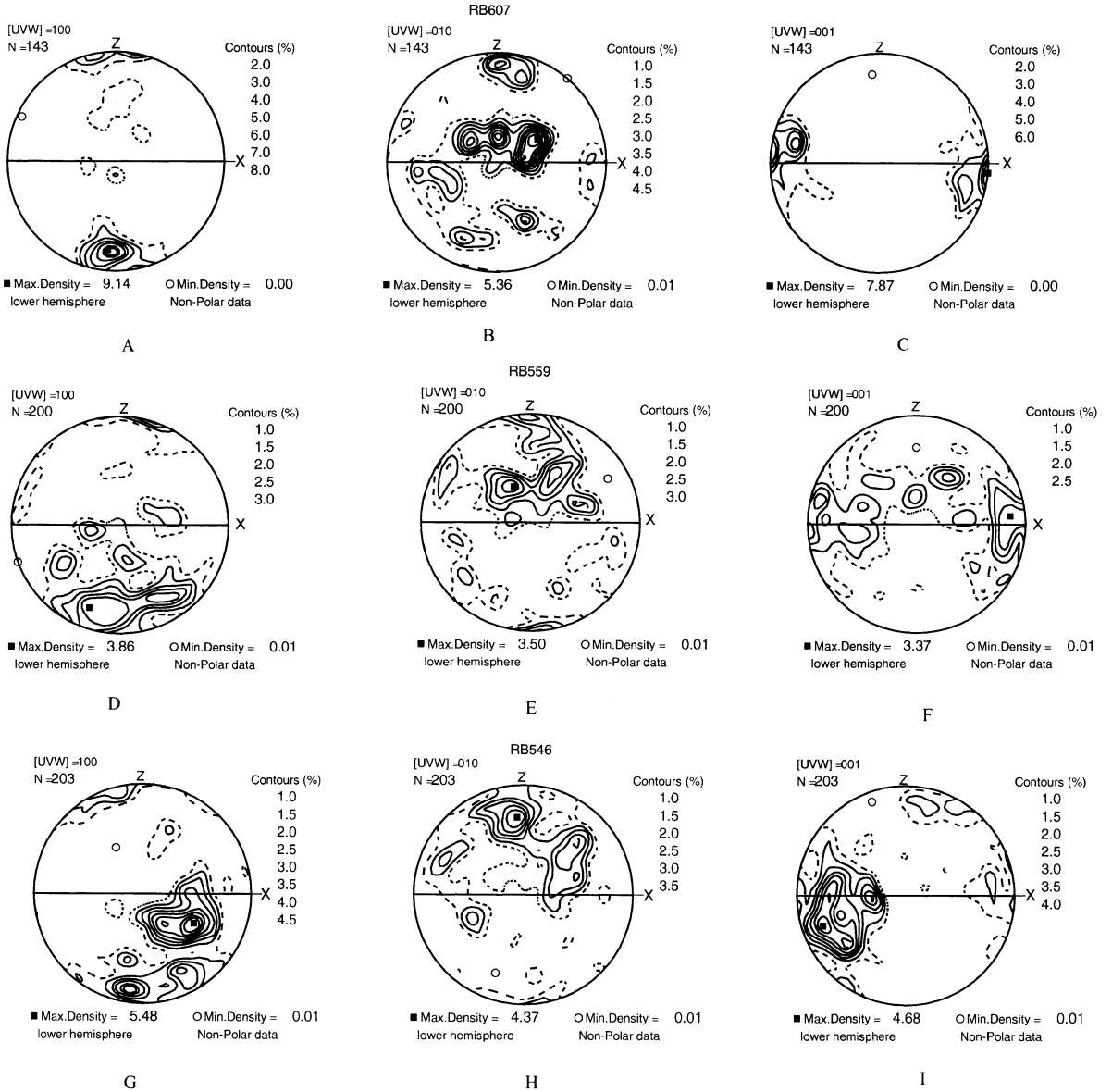

Fig. 15. Orthopyroxene lattice preferred orientations of granulite mylonites measured with the EBSD technique. Foliation (*XY* plane) is vertical and lineation (*X*) is horizontal.

9. Pyroxenes

Ortho- and clinopyroxene are 60–90 μm in size and show limited evidence of intracrystalline deformation. Orthopyroxene in mylonites and protomylonites typically forms trails of crystals that parallel the mylonitic stretching lineation. The larger grains frequently display slightly elongate shapes (Fig. 14B). Generally, orthopyroxene shows a strong preferred orientation with (100) oriented parallel to the foliation plane (Fig. 15A and D), [001] parallel to the stretching lineation (Fig. 15C and F) and clustering of [010] near the *Y* structural direction (Fig. 15B and E). Even outside the ductile shear zones (6–8 km away), orthopyroxene exhibits a relatively strong fabric. In this environment, [100] and [010] show some dispersion but still display clear concentrations. The highest density of [001] is always close to *X* structural axis.

Since (100) and [001] coincide with the flow plane and the flow direction, respectively, this LPO is likely due to the activation of the (100)[001] slip system. Dominant activation of the (100)[001] slip system in orthopyroxene was confirmed by TEM observations in experimentally and naturally deformed rocks in pioneering work on dislocations by Coe and Muller (1973) and Kohlstedt and Van der Sande (1973).

The strong orthopyroxene LPO observed in these high-temperature mylonites, characterized by parallelism of (100) with the foliation plane and [001] with the lineation, suggests that mylonitization occurred

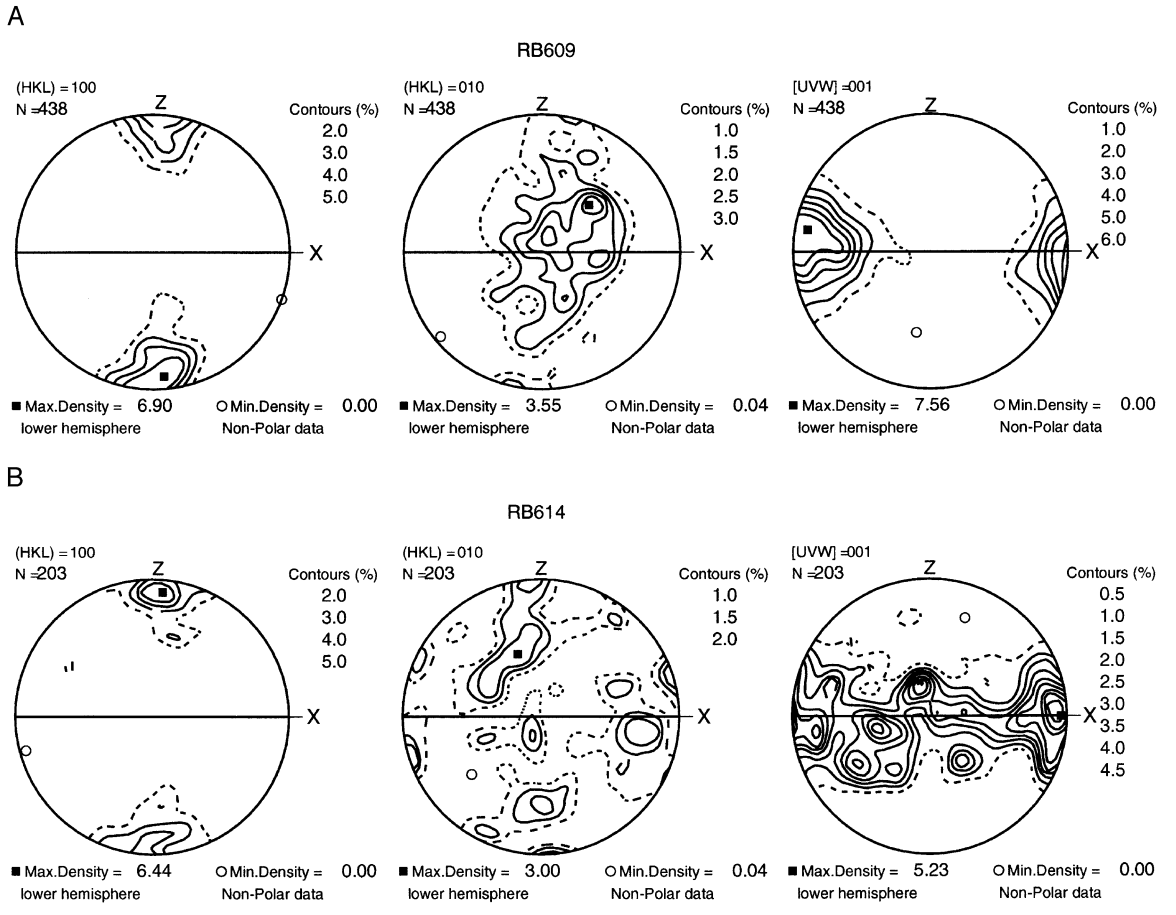

Fig. 16. Amphibole lattice preferred orientations of granulite mylonites measured with the EBSD technique. (A) Sample RB609 and (B) sample RB614. Foliation (*XY* plane) is E–W/vertical and lineation (*X*) is horizontal.

within the physical conditions of the pyroxene's plasticity, a conclusion in good agreement with available thermobarometric results ($T_{max} \cong 880$ °C at ± 700 MPa).

10. Amphibole

Amphibole usually exhibits large grains elongated in the foliation plane parallel to the macroscopic lineation. However, in a few cases, amphibole crystals are equidimensional, polygonal, and display 120° triple junction boundaries, forming part of a polymineralic matrix. Consistently, there is almost no substructure in amphiboles.

Amphibole LPOs are similar to those of orthopyroxene (Fig. 16A). The (100) poles are preferentially oriented close to the foliation pole, [001] clusters around the *X*-axis, and the (010) poles are dominantly located near *Y*. As for orthopyroxene, this amphibole LPO pattern suggests that slip occurred mainly through activation of the (100)[001] slip system (Rooney et al., 1975). Samples less deformed than the mylonites also exhibit a preferred orientation of the amphibole crystals. However, the (010) and (001) planes in these samples show a more complex distribution; [001] is spread in the foliation plane and (010) poles show a diffuse distribution (Fig. 16B).

Considering the microstructure and LPO of amphibole in the high-temperature mylonites, we suggest that this mineral deformed through dislocation creep assisted by diffusion. Dislocation creep and dynamic recrystallization likely account for LPO development, whereas diffusion accommodated recovery and grain growth.

11. Discussion and conclusion

The Ribeira belt resulted from the collision between the proto-South American and western African continents during the final amalgamation of western Gondwana (600–570 Ma). An anastomosing network of shear zones formed within the southern Ribeira belt due to the arcuate shape of the residual basin, and the presence of an old cratonic domain at the margin of the proto-South American continent. In the central domain of the belt, the Além Paraíba–Pádua dextral shear zone system contains mylonites deformed under granulite facies metamorphic conditions. Shear zones in the Pádua system are parallel to the regional tectonic trend and display evidence of deformation at higher temperature than the Além Paraíba shear zone. The Além Paraíba shear zone is slightly oblique to the regional orogenic trend; it represents a mega-scale C' shear band that acted as a strain transfer shear zone accommodating the orogen-normal contraction components in a transpressional regime.

A detailed study of the microstructures and LPO of mylonites outcropping in the APPSS provide insights on the mechanical behavior of the major mineral constituents of the granulite facies mylonites. Microstructure and LPO of plagioclase, orthopyroxene and amphibole demonstrate that these minerals have been deformed plastically through activation of intracrystalline slip systems characteristic of high-temperature conditions. This supports that mylonitization in the transcurrent shear zones started in the granulite facies under high-temperature conditions, a conclusion that agrees with a limited cooling of the crust during the transition from the earlier thrusting event to the transcurrent deformation (Porcher, 1997).

Quartz exhibits microstructural evidence supporting a major contribution of diffusion during and after mylonitization. Enhanced grain growth and static recrystallization deeply modified the microstructure after deformation ceased. This static evolution may have significantly modified the initial, syn-kinematic quartz LPO. As a result, it is unclear if the observed quartz LPO was retained from the syn-kinematic evolution, thereby hindering any interpretation of LPO patterns in terms of deformation mechanisms active during mylonitization. Quartz LPO displays an evolution from the border to the core of shear zones. LPOs with a point maximum of [0001] axis close to the *Y* structural direction dominate in the external domain of the shear zones. In the internal domains, the maximum density tends to spread between the *Y* and *Z* directions, and in the core of the shear zone, quartz LPOs usually display point maxima symmetrically located either between *Y* and *Z*, or between *Z* and *X*. The latter LPO seems to characterize samples in which diffusion processes continued after deformation leading to static transformation of the syn-kine-

matic microstructure. This across-strike microstructural and textural evolution of quartz might be an effect of a thermal gradient across the shear zone, the central, more deformed domain being also hotter than the periphery. Such a temperature variation across the shear zone might have resulted in the periphery and in the core of the shear zones being respectively in the field of stability of the α- and β-quartz during the last increments of deformation and the subsequent post-kinematic annealing.

The LPO of orthopyroxene, plagioclase, and amphibole support that these minerals have been deformed through dislocation creep with the activation of the (100) [001] slip system in orthopyroxene and amphibole, and of the (010) [001] and (010) [100] slip systems in plagioclase. Evidence of intracrystalline slip in these minerals, of mechanical twinning and pervasive recrystallization in plagioclase, and of extensive grain boundary migration in quartz points toward transcurrent deformation starting under very high-temperature conditions, probably >800 °C. In the southern domain (southern Além Paraíba fault), remnants of granulitic mylonites embedded in migmatitic mylonites suggest that the deformation continued during cooling down to the upper amphibolite facies, but the lack of any evidence of low-temperature reworking suggests that strike-slip faulting stopped before the geotherm returned to normal.

Acknowledgements

This research was supported by (FAPESP, project. 95/0283-3, CAPES/COFECUB project 287/99 and CNPq/CNRS, project 910144/98-2). We thank the National Laboratory of Synchrotron Light (LNLS) at Campinas-SP for the use of Scanning and Transmission Electron Microscopy facilities. Thanks are due to D. Mainprice and G. Barruol for their involvement in the development of a SEM-EBSD system at the Laboratoire de Tectonophysique, Montpellier. This development was made possible through funding by the INSU-CNRS, the University of Montpellier II, and the National Science Foundation (project #EAR-9526840 ''Anatomy of an Archean craton''). We also acknowledge the constructive comments of Benito Ábalos and Luis Eguiluz Alarcón that have improved the final version of the manuscript and Brendan Murphy for English improvements.

References

Adams, B.L., Wright, S.I., Kunze, K., 1993. Orientation imaging: the emergence of a new microscopy. Metall. Trans. 24A, 819–831.

Brueckner, H.K., Cunningham, D., Alkmin, F.F., Marshak, S., 2000. Tectonic implications of Precambrian Sm–Nd dates from the southern São Francisco craton and adjacent Araçuaí and Ribeira belts, Brazil. Precambrian Res. 99, 255–269.

Bunge, H.J., Wenk, H.R., 1977. Three-dimensional texture analysis of three quartzites (trigonal crystal and triclinic specimen symmetry). Tectonophysics 40, 257–285.

Coe, R.S., Muller, W.F., 1973. Crystallographic orientation of clinoenstatite produced by deformation of orthoenstatite. Science 180, 64–66.

Dingley, D.J., Field, D.P., 1997. Electron backscatter diffraction and orientation imaging microscopy. Mater. Sci. Technol. 13, 69–78.

Egydio-Silva, M., Mainprice, D., 1999. Determination of stress direction from plagioclase fabrics in highgrade deformed rocks (Além Paraíba shear zone, Ribeira fold belt, southeastern Brazil). J. Struct. Geol. 21, 1751–1771.

Green, H.W., Griggs, D.T., Christie, J.M., 1970. Syntectonic and annealing recrystallization of fine-grained aggregates. Experimental and Natural Rock Deformation. Springer-Verlag, Berlin, pp. 272–335.

Haralyi, N.L.E., Hasui, Y., 1982. The gravimetric information and Archean–Proterozoic framework of eastern Brazil. Rev. Bras. Geocienc. 112, 160–166.

Heillbronner, R., Tullis, J., 2001. Effect of static annealing on microstructures and CPO of quartzites deformed in axial compression and shear. Deformation Mechanisms, Rheology and Tectonics. Universiteit Utrecht, Utrecht, p. 68.

Helming, K., Wenk, H.R., Choi, C.S., Schafer, W., 1994. Description of quartz textures by components. Examples from metamorphic rocks. In: Bunge, H.J. (Ed.), Textures in Geological Materials. Obersursel, Germany, pp. 303–325.

Hobbs, B.E., 1968. Recrystallization of single crystal of quartz. Tectonophysics 6, 353–401.

Humphreys, F.J., Hatherly, M., 1995. Recrystallization and Related Annealing Phenomena Pergamon, Oxford, 497 pp.

Ji, S., Mainprice, D., 1988. Natural deformation fabrics of plagioclases: implications for slip systems and seismic anisotropy. Tectonophysics 147, 145–163.

Ji, S., Mainprice, D., 1990. Recrystallization and fabric development in plagioclase. J. Geol. 98, 65–79.

Kohlstedt, D.L., Van der Sande, J.B., 1973. Transmission electron microscopy investigation of the defect microstructure of four natural orthopyroxenes. Contrib. Mineral. Petrol. 42, 169–180.

Lloyd, G.E., Schmidt, N.H., Mainprice, D., Prior, D.J., 1991. Crystallographic textures. Mineral. Mag. 55, 331–345.

Machado, N.V.C., Heilbron, M., Valeriano, C., 1996. U–Pb geo-

chronology of the central Ribeira belt (Brazil) and implications for the evolution of the Brazilian orogeny. Precambrian Res. 79, 347–361.

Mainprice, D., Bouchez, J.L., Blumenfeld, P., Tubía, J.M., 1986. Dominant *c* slip in naturally deformed quartz: implications for dramatic plastic softening at high temperature. Geology 14, 819–822.

Masuda, T., Morikawa, T., Nakayama, Y., Suzuki, S., 1997. Grain boundary migration of quartz during annealing experiments at HT and P, with implications for metamorphic geology. J. Metamorph. Geol. 15, 311–322.

Nicolas, A., Poirier, J.P., 1976. Crystalline Plasticity and Solid State Flow in Metamorphic Rocks Wiley, London, 444 pp.

Olsen, T.S., Kohlstedt, D.L., 1984. Analysis of dislocations in some naturally deformed plagioclase feldspar. Phys. Chem. Miner. 11, 153–160.

Passchier, C.W., Trouw, R.A.J., Zwart, H.J., Vissers, L.M., 1992. Porphyroblast rotation: eppur si muove. J. Metamorph. Geol. 10, 283–294.

Pedrosa-Soares, A.C., Vidal, P., Leonardos, O.H., Brito Neves, B.B., 1998. Neoproterozoic oceanic remnants in eastern Brazil: further evidence and refutation of an exclusively ensialic evolution for the Araçuaí–West Congo orogen. Geology 26, 519–522.

Porcher, C.C., 1997. Relationships between metamorphism and deformation in Ribeira belt: Três Rios and Santo Antônio de Pádua region (RJ), eastern Brazil. unpublished PhD thesis, UFRGS, Porto Alegre, Brazil.

Rooney, T.P., Riecker, R.E., Gavasci, A.T., 1975. Hornblende deformation features. Geology 3, 364–366.

Schmid, S.M., Casey, M., 1986. Complete fabric analysis of some commonly observed quartz *c*-axis patterns. In: Heard, H.C., Hobbs, B.E. (Eds.), Mineral and Rock Deformation, Laborat. Studies—The Paterson Volume. Geophys. Monogr., vol. 36. American Geophysical Union (AGU), Washington, pp. 263–286.

Schmidt, N.H., Olesen, N.Ø., 1989. Computer-aided determination of crystal-lattice orientation from electron-channeling patterns in the SEM. Can. Mineral. 27, 15–22.

Söllner, F., Lammerer, B., Weber-Diefenbach, K., 1991. Die Krustenentwicklung in der Kustenregion nordlich von Rio de Janeiro/Brasilien. Munch. Geol. Hefte 4, 1–101.

Starkey, J., 1979. Petrofabric analysis of Saxony granulites by optical and X-ray diffraction methods. Tectonophysics 58, 201–219.

Vauchez, A., 1987. The development of discrete shear-zones in a granite: stress, strain and changes in deformation mechanisms. Tectonophysics 133, 137–156.

Vauchez, A., Tommasi, A., Egydio-Silva, M., 1994. Self-indentation of a heterogeneous continental lithosphere. Geology 22, 967–970.

Vauchez, A., et al., 1995. The Borborema shear zone system. J. South Am. Earth Sci. 8, 247–266.